AIAA 2013-2285

Noise from a Rotor Ingesting a Planar Turbulent Boundary Layer

W. Nathan Alexander[1], William Devenport[2], and Michael A. Morton[3]
Virginia Tech, Blacksburg VA 24061

Stewart A. L. Glegg[4]
Florida Atlantic University, Boca Raton FL 33431

This study concerns rotor noise generated by the ingestion of anisotropic, inhomogenous turbulence produced by a planar turbulent boundary layer. Far field noise was recorded at multiple receiving angles and blade wake profiles were measured for advance ratios ranging J=0.48 to 1.44. A novel method to infer the turbulence characteristics from the measured far field noise is presented. The time-frequency distribution of the recorded noise is used to estimate the streamwise scale of the turbulence while the time-averaged spectra are used to estimate the lateral scale. Results show that the estimated streamwise scale doubles over the measured range of advance ratios and the lateral scale remains approximately constant. This suggests a complex distortion of the turbulence due to the sheared flow and presence of the wall, a topic addressed in a companion paper (Glegg *et al*., 2013).

I. Introduction

Rotors produce noise by many different aerodynamic mechanisms including leading and trailing edge noise as well as periodic shedding noise, but their rotational character also introduces some unique acoustic characteristics. These include blade slap, Gutin noise, and haystacking. This paper focuses specifically on the last characteristic, haystacking. Haystacking is a broadband phenomenon around the blade-passing-frequencies (BPFs) due to the correlated cutting of turbulent structures by successive blades.

Sevik (1971) was one of the first to study the noise produced by turbulence ingestion into a rotor. The turbulence was grid-generated and was assumed isotropic and homogeneous. He measured the spectral noise using a 10-blade rotor with 25.4mm chord and 203.2mm diameter spinning at 1100RPM with an inflow velocity of 4.6m/s. He was the first to observe these haystacks around the BPFs, but because he neglected blade-to-blade correlations in his theory, predictions omitted the haystacking phenomenon.

Hanson (1974) conducted a study which focused on the ingestion of atmospheric turbulence into a ducted fan during static and flight conditions. During static tests, the turbulent eddies in the atmosphere are stretched very thin and long as they enter the rotor plane and are therefore cut many times by successive blades producing coherent unsteady blade loading. The resulting noise can be narrow band and is often confused with the noise from fixed flow distortion. Hanson provides a theoretical explanation of haystacking noise derived from a train of enveloped blade loading lift pulses with finite length taking into account both slight random variations in pulse position and pulse amplitude. He finds that the random pulse position has an effect on the predicted spectral peaks reducing them with increasing frequency while the energy is displaced to a broadband component. The variations in pulse amplitude also contribute a broadband component.

Majumdar & Peake (1998) also theoretically analyzed the distortion of isotropic turbulence as it is ingested into an engine. They also showed that during static tests eddies are stretched significantly in the streamwise direction and are cut by multiple blades producing broadband far field tones. Both Hanson's (1974) and Majumdar & Peak's (1998) analyses show that this stretching is considerably larger under static conditions than flight conditions due to the greater contraction of the streamtube leading into the fan face. Also, it was shown that the blade-to-blade coherence, and therefore tonal noise, increases with the integral lengthscale of the turbulence since larger eddies interact with a larger number of blade passes.

[1] Research Scientist, Department of Aerospace and Ocean Engineering, AIAA Member.
[2] Professor, Department of Aerospace and Ocean Engineering, AIAA Associate Fellow.
[3] Wind Tunnel Test Engineer, Department of Aerospace and Ocean Engineering, AIAA Member.
[4] Professor, Department of Ocean and Mechanical Engineering, AIAA Associate Fellow.

Wojno *et al*. (2002, 2002a) used the 10-bladed Sevik rotor to measure the noise from grid-generated turbulence. In these studies, they measured the undisturbed velocity characteristics downstream of three grids with various mesh sizes to define spatially averaged semi-empirical turbulence models used to simulate the ingested flowfield of their rotor. Noise from the rotor was measured and compared to predictions that use the turbulence models to estimate the level of coherence between blades to resolve the haystacks. Their predictions use the summation gain approach described in Blake (1986) which estimates the coherence using the defined turbulence scales and blade spacing. Their predictions peaked at frequencies below the first BPF and underpredicted the peaks at all BPFs suggesting that the combined turbulence model and summation gain approach did not accurately represent the coherent fluctuating loads between blades.

These previous studies, while advancing the knowledge of the haystacking phenomenon, all used the assumption of isotropic turbulence. Stephens & Morris (2009) extended the topic by measuring noise from the Sevik rotor in anisotropic flow by placing it in a 206mm diameter duct. They adjusted the thickness of the wall boundary layer by placing the rotor at various streamwise positions in the duct which allowed the effect of the turbulent boundary on the sound to be studied independently of any self-noise. A subset of the two-point velocity correlation matrix was measured at one location 1.125 rotor diameters downstream of the inlet where the boundary layer thickness was 11mm. A simple model was used to extrapolate this data to the complete four-dimensional correlation matrix and was scaled to the other streamwise duct locations using measured momentum thicknesses. They used the correlation matrix to make predictions of the noise produced by the rotor using strip theory and showed good agreement with their acoustic measurements. Their analysis demonstrates that a reliable prediction of rotor noise can be made if an accurate description of the turbulence space-time correlation is known.

Many studies focus on the ingestion of anisotropic flow by ducted fans where often thin boundary layers exist axisymmetrically about the rotor, but a recent study by Catlett *et al*. (2012) measured the sound produced by a rotor centered downstream in the sheared flow behind a 3.05m chord airfoil. In this case, the rotor blades pass through the wake of the airfoil. They clearly measured the haystacking phenomenon but also propose the topic of the non-stationary aspects of the noise source. Since the inflow is spatially inhomogeneous, they suggest that the produced noise varies according to blade position.

This study is concerned with the noise produced by the ingestion of anisotropic inhomogeneous flow, specifically a two-dimensional planar boundary layer. This would be analogous to the conditions seen by an embedded engine on blended-wing-body (BWB) aircraft. Although, there are many studies concerning rotors, none have specifically addressed this type of turbulent inflow. This study is an extension of a previous experiment described in Morton *et al.* (2012) which details measurement of the undisturbed boundary layer flow including the complete four-dimensional velocity correlation matrix. A companion to the present paper (Glegg *et al*., 2013) addresses the distortion of the ingested turbulence using a modified form of classical rapid distortion theory. This paper presents the analysis of an experiment in which a 2.25 scaled version of the Sevik rotor was immersed in the boundary layer described in Morton *et al*. (2012) while synchronous blade position and far field sound were recorded at advance ratios ranging 0.48-1.44. Boundary layer profiles and the blade wakes downstream of the rotor were also measured. This is the first time that broadband noise due to the ingestion of inhomogeneous turbulence into a rotor has been studied in which the full linear inflow boundary condition has been known. The study is therefore expected to yield new insight into turbulence distortion by a rotor, broadband noise generation, and the mathematics of inhomogeneous turbulence interaction.

II. Apparatus and Instrumentation

A. Wind Tunnel

Data were taken in the Virginia Tech Stability Wind Tunnel which has low turbulence levels (0.01% to 0.03%) and interchangeable aerodynamic and anechoic test sections each 1.83m square and 7.3m long. The anechoic section, detailed in Devenport *et al*. (2013), has tensioned Kevlar walls which are acoustically transparent but contain the flow so a jet catcher is not needed. Acoustic data can be taken from anechoic chambers that run alongside the test section on the port and starboard side. The floor and ceiling of the anechoic section are made of Kevlar stretched over perforated panels. Behind these panels are acoustic foam wedges to dampen reflections. For this study, the starboard Kevlar wall was replaced with six equal size Lexan panels that extended the entire length of the test section and reduced the test section width by 0.12m. A 2.4m long curved fairing placed in the contraction section of the tunnel smoothed the discontinuity between the tunnel and Lexan wall. A diagram of the modified test section is shown in Figure 1. This modified configuration has been used in several other studies (Morton, 2012, Forest, 2012, Awasthi, 2012) to grow high Reynolds number thick boundary layers. A single 9.5mm trip was placed 4.76m upstream of the rotor in the contraction section resulting in the growth of a two-dimensional boundary layer

on the false wall approximately 100mm thick at the location of the rotor plane with Re_θ up to 16,600. The wall location is adjustable and was positioned to produce a zero pressure gradient by measuring the streamwise variation of the static pressure on the test section floor and ceiling. The inflow conditions for all tested free stream velocities are shown in Table 1 and were compared to the previous companion study of Morton *et al.* (2012) for consistency. Due to error in the measurement, the boundary layer thickness for the 15m/s case has been interpolated from the results for the 10m/s and 20m/s cases.

Table 1. Boundary layer characteristics upstream of rotor

U_∞, m/s	δ, mm	δ*, mm	θ, mm
10	102.2	15.2	10.0
15	101.2	15.0	10.1
20	100.1	14.0	9.3
30	99.7	13.3	8.9

B. Rotor

The rotor was a 2.25 scale version of the rotor used in Sevik's (1971) study. It has 10-blades with 57.2mm chord and a tip diameter of 457.2mm. The hub diameter was extended slightly beyond the 2.25 scale to a 127mm diameter by removing the inner 6.35mm of each blade root. The blades have square tips and no skew. The geometric angle of attack varies from 55.6° at the root to 21.2° at the tip. The airfoil sections have a maximum thickness of 9.7% at the root and 8.4% at the tip occurring approximately at mid-chord. Sevik indicates that the design advance ratio for this rotor is 1.17. The nose of the rotor was extended to house instrumentation although no on-board devices were used in this study. A straight, constant-diameter 247.1mm long instrumentation tube extended in front of the rotor blade sections which was capped by a 135.6mm long aerodynamic nose cone. Photos of the rotor can be seen in Figure 2. The rotor was powered using a Kollmorgen AKM-64P-ACCNDA00 servo-motor and S61200 servo-drive. The tip gap was 20.3mm at the closest approach of the blade tips to the false wall so that approximately 80mm of the rotor disk was immersed in the wall boundary layer.

C. Microphones

Bruel & Kjaer ½" microphones were used to record the noise produced by the rotor. Two microphones were positioned in the flow using ½" Bruel & Kjaer bullet nose caps. The inflow microphones were held by stands with airfoil shaped cross-sections designed to produce low noise levels. Four microphones were positioned in the port chamber behind the Kevlar window in an arc pointing at the rotor hub. All of the measured microphone positions are shown in Figure 1b and positions are given in Table 2 with reference to the center of the rotor plane, x is streamwise distance upstream, y is away from the Lexan wall, and z is spanwise across the wall to complete the right-hand rule. The inflow microphone at Pos. 1 remained at this location during all inflow measurements. The second inflow microphone was moved during testing between locations Pos. 2, 3, 8, and 9. Corresponding background noise measurements were made for each inflow microphone position to remove the stands' contribution to the far field. Background noise measurements also included the motor noise and the aerodynamic noise produced by the motor housing. These background measurements were made by operating the rotor with the blade section removed.

Data were recorded with B&K Pulse 14 software and a series of synchronized 3050-A LXI data acquisition systems sampling at 65536Hz for 32 seconds for each measurement. The presented frequency-spectra are the average of 511 records of 8192 samples each taken from these records. Multiple data sets from the same inflow and rotor conditions have been averaged to further reduce uncertainty. These data were all synchronized with the measurement of blade position using the photodiode system described below.

Table 2. Microphone positions relative to rotor

	Pos. 1	Pos. 2	Pos. 3	Pos. 4	Pos. 5	Pos. 6	Pos. 7	Pos. 8	Pos. 9
x, mm	2172	2122	2116	1081	662	332	0	-1529	-2746
y, mm	569	562	1175	2243	2731	3119	3350	1183	570
z, mm	152	-94	-94	-88	-90	-85	-73	-94	-94
θ, deg	15	15	29	64	76	84	90	142	168

D. Laser/Photodiode

A laser system was used to record blade position by pointing the laser through the blade plane at a photodiode adhered to the backside of the upstream wall. The laser was positioned on the side of the rotor motor housing and passed through the blades at approximately 90% radius. This set-up is shown in Figure 3. The photodiode's sensitivity was adjusted so that its output response resembled a square wave with the passing of each blade. The absolute position of individual blades was not recorded since the rotor phase repeats every 36° for the 10 evenly spaced blades. These position data allow the far field microphone measurements to be phase averaged with blade position for analysis of the time varying component of the signal. The photodiode response signal was recorded simultaneously with the microphone data using the 3050-A LXI DAQs at 65536Hz. This gives sufficient resolution to resolve every 0.25° at the highest studied rotational velocity 2734RPM. The blade-position signal was also measured simultaneously with wake profiles measured with a four-sensor hotwire probe using an Agilent E1432 16-bit digitizer at 51200Hz

E. Hotwire

A four-sensor hotwire probe was used to measure boundary layer profiles 789mm upstream of the rotor blades. The hotwire was traversed vertically from 8.5mm to 152mm approximately 1.2 times the boundary layer thickness. There were 30 logarithmically spaced measurement locations in each profile. The probe was also used to make phase-locked measurements of the blade wakes 36.5mm downstream of the rotor. The blade wake profiles were measured at a single stationary point located 43mm from the wall (at 90% of the blade radius) so that the leading edge of the blade passed in front of the hotwire at 4.9° of rotation before bottom dead center. For all measurements the probe stem axis was parallel to the wall.

The probe is composed of four sensors each nominally 45° from the streamwise axis arranged in a square pattern so that each sensor is perpendicular to the two adjacent sensors. Four sensor probes provide redundant measurement of the three components of the velocity field which minimizes velocity gradient errors. The sensors are 5μm tungsten wire 1.2mm long so that the measurement volume is approximately 0.75mm^3. Angle calibrations were performed on the probes in low turbulence jet prior to the wind tunnel measurement and were applied to data using the look-up table method of Wittmer *et al.* (1998). Velocity calibrations were conducted during the experiment to account for changes in the environmental operating temperature. The probe was operated with a Dantec Streamline anemometer and data were recorded using an Agilent E1432 16-bit digitizer. Boundary layer data were sampled at a minimum of 6400Hz. Single point measurements downstream of the rotor were sampled at 51200Hz for 32 seconds.

III. Results and Discussion

Figure 4 shows the typical signal-to-noise ratio (SNR) for the inflow measurement at 15° (Pos.1), which was the most advantageous measured receiving angle for a streamwise aligned dipole, and a port-side chamber measurement at 90° (Pos. 7) for the highest and lowest studied rotational velocities. At 1000RPM, the SNR was similar for both locations at 7dB. For the higher rotational velocity case, 2734RPM, the haystacking phenomenon is clearly measured at both locations, but the SNR of the first BPF at 15° is over ten times that of the measurement at 90°. All of the following figures of the mean spectra will be presented with tunnel background noise subtracted using a minimum discretion level of 1dB.

The measurement of haystacks at 90° is a significant result in itself showing that the directivity pattern is not a simple dipole and that the results in the rotor plane cannot be ignored. The analysis of Morton (2012) explains the observed complex directivity pattern as a function of the twist in the blades which will radiate a component of the fluctuating force in the rotor plane. The coherence between the acoustic signals and the blade position was observed to be zero in the haystacks suggesting that the measured noise is due to the ingestion of turbulence which is statistically random process and not tone noise associated with mean-flow non uniformity. This turbulence noise should only be expected to correlate over very short time periods as multiple blades cut through the same turbulent structure.

Figure 5 shows the measured directivity pattern for the U_∞ =15m/s, 2734RPM case. These data have been corrected to equal radial distance from the source. As the receiving angle increases, the strength of the haystacks decreases monotonically. Figure 5b isolates the 15º and 90º curves to show that the haystacks peak at the BPF and its harmonics, but they are right-skewed meaning most of the area is under the high frequency side of the haystack. Glegg *et al.* (2012) predict a slight right peak shift and skew in the haystacks and show that as the ratio of tip Mach number to axial Mach number increases that the haystacks become more symmetrical. This effect is shown in Figure 6 as the rotational velocity is held constant and the inflow speed adjusted from 10m/s to 30m/s. The haystacks

become narrower and more symmetric as the value of J, the advance ratio, decreases. Also, as J decreases, the number of observable haystacking harmonics increases. The large broadband hump centered around 9kHz for the 20m/s and 30m/s cases appears to be due to vortex shedding at small angles of attack, a source studied in many papers including Hersh *et al.* (1974) and Paterson *et al*. (1973).

The haystacking phenomenon is believed to occur because of the correlated cutting of turbulent structures by successive blades. Therefore, the produced far field noise should reflect the characteristics of the turbulent structures in the flow as they stretch and pass through the rotor plane. Starting with this premise, the noise variation with time was analyzed using a short-time Fourier transform approach in order to isolate the noise created by the rotor interaction with independent flow structures. Figure 7 shows the spectrograms produced through this analysis for three different example conditions varying both inflow velocity and rotational velocity independently. These spectrograms were calculated with record lengths of 1025 samples centered at each time step. The results were then averaged over 0.0022s to remove artifacts of the analysis technique that have shorter duration than a single blade pass. Figure 7 shows that noticeable fluctuations are present in the far field noise produced at the blade passing frequency that extend over time periods longer than a single blade passage. These fluctuations are responsible for the time-averaged quantities shown in the mean spectra of Figures 4 to 6 and do not have a periodic nature that would suggest a mechanical noise source linked to the absolute rotational position of the rotor. The fluctuations appear and disappear randomly in time and have varying time scales. This suggests the fluctuations may be due to the ingestion of the turbulent structures in the flow. Specifically, the passage time of the noise fluctuations would correspond to the streamwise lengthscale of the turbulence. If the rotor is assumed to uniformly accelerate and stretch the turbulence into the rotor plane, the observed passage timescale of the turbulence recorded in the far field would be equivalent to the passage timescale of a coherent structure being convected in the undisturbed boundary layer.

To determine the implied streamwise lengthscale at each condition, a time series was constructed using the mean of the nearest three frequency bins bounding the BPF. The time autocorrelation for each condition was determined as the average of 29 records each 1.06s in length. The time autocorrelations for all of the measured conditions which produce observable haystacks are shown in Figure 8. Generally, the width of the main lobe around zero time delay decreases as the advance ratio increases except for the J=0.52 and J=0.66 cases. These cases also do not approach zero with increasing time delay, but instead have a fluctuating component of the correlation corresponding to the once per revolution rotation rate of the rotor. This suggests that there may be some level of mechanical noise observable at these frequencies for these two conditions. The integral timescale was calculated from the autocorrelations by integrating the area under each curve between the intersections with a coherence level of 0.5. The calculated normalized lengthscales, x/δ, or equivalently normalized timescale, tU_∞/δ where t is the determined integral timescale, for each of these conditions are shown in Figure 9. Surprisingly, the streamwise timescales double over the measured range of advance ratios from tU_∞/δ =1 to tU_∞/δ =2. Similarity between the measured undisturbed boundary layers for all inflow velocities infers that the undistorted streamwise timescale would remain approximately constant. Also, for each inflow velocity, there is a trend of decreasing timescale with decreasing rotational speed. The effect of rotational velocity on the determined streamwise timescale decreases as J increases towards the zero-thrust condition J=1.44. This observation suggests that the turbulence distortion may be more complex than can be computed using simple actuator disk theory without the presence of the wall in which the normalized timescale would be expected to remain constant. A companion paper (Glegg *et al*., 2013) addresses the complex distortion of the ingested turbulence using rapid distortion theory modified so that it is applicable in sheared flow. Direct comparison of the measured and predicted turbulence timescales are presented in their paper.

The lateral scale of the turbulence may be inferred from the peak decay of the haystacks in the far field mean pressure spectra for each case. Figure 10 shows the far field noise recorded at a receiving angle of 64° for J=0.72. As stated before, the haystacking phenomena is a result of a periodic cutting of coherent structures by successive blades causing unsteady loads which radiate to the far field. This unsteady loading can be observed in the far field as a periodic train of functions that correlate to the blade response with respect to the turbulence. If the blade response is assumed to relate to the ingested turbulence, the mean lateral scale of the turbulence can be inferred by fitting the Fourier transform of the function that is periodic with the blade passage time to the mean far field spectra. For this analysis, a Gaussian blade loading response function was used to approximate the time unsteady blade loading function. The Fourier transform of a train of Gaussians is a train of impulses at the occurrence frequency and its harmonics whose peak values decay as a Gaussian. The width of the Gaussians was determined by fitting the decay from the BPF to its n=2 harmonic. The Gaussian fit for the J=0.72 case is shown in Figure 10 along with the experimental data and the spectrum calculated for a periodic train of impulses at the blade passage frequency. The effect of the blade response function is apparent when comparing the train of impulses to the train of Gaussians. The shape of the blade loading turbulence response function, which produces the periodic far field noise due to the

unsteady loading, determines the decay rate. Also, Figure 10 shows that the Gaussian is not an ideal fit to this function as it decays too rapidly with frequency increasingly underpredicting the magnitude of the 3rd, 4th, and 5th harmonics.

Acknowledging this flaw, the Gaussian was used to approximate a mean lateral timescale using the full width at half maximum (2.35σ) multiplied by the blade velocity at 95% radius for all of the cases in which the haystacking phenomenon was clearly observed in the mean spectrum. The results are shown in Figure 11 showing little variation with advance ratio. The calculated lateral scale shows some dependence on the rotational speed decreasing with increasing RPM. This is the inverse of the trend as observed in the streamwise lengthscale shown in Figure 9, but for the calculated lateral scale, the variation is to a much lesser extent varying by only 10%δ. Further analysis on the mean lateral dimension is being conducted using the measured time data in which intermittent periodic fluctuations are easily observed at the blade passage rate. Also, direct measurements of the ingested turbulence are planned shortly using hotwire anemometry fixed to blades in the rotational frame to measure unsteady upwash velocities.

Although direct measurements of the inflow turbulence from the perspective of the rotor blades have yet to be performed, phase averaged turbulence quantities of the blade wakes were measured. Fixed location hotwire measurements were made in the wall coordinate system 0.64 chord lengths downstream of the trailing edge at a location 43mm away from the wall phase locked with the rotor rotation. Mean velocity measurements are shown in Figure 12 and mean Reynolds normal stress profiles are shown in Figure 13 for cases of decreasing *J*, holding the free stream velocity constant at U_∞=15m/s. The horizontal axis is measured in degrees corresponding to the physical location of the leading edge of the rotor blades with the 0º reference to a line normal to the wall. The normal Reynolds stress quantities increase in the blade wake and between wakes for the high thrusting cases. Also, with increasing thrust the $\overline{w^2}$ and $\overline{v^2}$ stresses increase above the $\overline{u^2}$ values notably for phase values between blade wakes. This may be due to the slight off-centerline location of the measurement combined with the effect of the flow directing itself into the rotor plane and the rotational component being added to the mean flow as it passes through the rotor plane.

Figure 14 shows the Reynolds shear stresses for the same cases. This progression shows that as the rotor thrust increases so does the boundary layer mixing in the wake as observed in increases in $\overline{uv}$. For the near zero-thrust case (*J*=1.31) the turbulence quantities between wakes are very near the undisturbed boundary layer values. The $\overline{uw}$ component shows mixing in the blade wake as lower streamwise velocity fluid with a strong rotational component -*W* mixes with the free stream flow between blades. As the advance ratio decreases, the $\overline{uw}$ component continues to show mixing on either side of the wake, but the center profile of the wake inverts because the fluid at the core of the wake has a slightly higher *U* component than the edges of the wake. It is unclear if this indicates that the flow is separating from the blade and higher velocity fluid is being entrained into the center of the wake. Measurements are needed at locations closer to the trailing edge of the blades.

Predictions of the rotor noise are compared to measurement in Figure 15. The predictions use the theory presented in Glegg *et al.* (2013) modified to include the image source in the wall and reformulated to solve the acoustic propagation of sources in the time domain. The time domain approach reduced the computational time from approximately 20 hours to 40 minutes. Their theory includes account of the rotor geometry including twist and uses the turbulence cross-correlation function to calculate the correlated unsteady loading of the rotor blades using a strip-theory approach and two-dimensional Sears function. Their theory is given in Equation 1.

$$S_{pp}(\mathbf{x},\omega)=\left(\frac{1}{4\pi T}\right)\sum_{n=1}^{B}\sum_{m=1}^{B}\int_{R_{hub}}^{R_{tip}}\int_{R_{hub}}^{R_{tip}}\int_{-T}^{T}\int_{-T}^{T}R_{FF}^{(n,m)}(R,R',\tau,\tau')\times\left\{\frac{\partial}{\partial x_i}\frac{n_i^{(n)}(R,\tau)e^{i\omega r^{(n)}(\tau)/c_o}}{4\pi r^{(n)}(\tau)}\right\}\left\{\frac{\partial}{\partial x_i}\frac{n_j^{(m)}(R,\tau')e^{-i\omega r^{(m)}(\tau')/c_o}}{4\pi r^{(m)}(\tau')}\right\}e^{i\omega(\tau-\tau')}dRdR'd\tau d\tau' \quad \text{Eq. 1}$$

where S_{pp} is the noise heard by an observer at **x**, *B* is the number of blades, *R* is the blade radius, R_{FF} is the surface loading correlation function, and the terms in curly brackets are the source propagation terms as functions of time. R_{FF} was determined using the measured undisturbed 4-D velocity cross-correlation function of the turbulent boundary layer presented in Morton *et al.* (2012) which was modified using the rapid distortion theory approach described in Glegg *et al*. (2013) to account for the distortion of the inflow for various operational conditions.

Therefore, the presented predictions do account for distortion of the turbulence into the rotor. Predicted noise is compared to the sound recorded at the zero-thrust condition (J=1.44) and a thrusting condition (J=0.72). These are non-absolute predictions and therefore only spectral shape should be compared. The predictions accurately reproduce the narrowing of the haystacks as the thrust is increased. Also, the predictions reproduce the increased number of harmonics observed as the advance ratio decreases. In both prediction and measurement, five haystacks are observed for J=0.72 and three haystacks are observed for J=1.44. There are some discrepancies between the prediction and measurement though. The haystack peaks decay differently between measurement and prediction. For the non-thrusting case (J=1.44), the haystacking peaks tend to decay slower in prediction, 9dB from the first to third harmonic, than observed in measurement, 14db from the first to third harmonic. The opposite is true for the thrusting case (J=0.72). The haystacking peaks decay more rapidly with frequency in the prediction, 18dB from the first to fifth harmonic, than the measurement, 15dB from the first to fifth harmonic. The prediction also does not accurately capture the observed right skew of the measured spectrum for the J=0.72 case in which the predicted haystacks are near symmetric about the BPF and its harmonics while the measured haystacks are significantly right skewed. Theoretical analysis of this problem continues with improved modeling of the rotor inflow using RANS since it has been modeled with a potential flow code for these calculations.

IV. Conclusions

Measurements of the sound and flow produced by an idealized 10-bladed rotor partially immersed in a thick plane turbulent boundary layer have been made for a range of advance ratios and flow speeds. This is the first time ingestion noise has been studied coupled with complete measurement of the four-dimensional two-point correlation matrix so that the character of the inhomogeneous anisotropic flow is known. Haystacks in the broadband noise spectrum, produced by the multiple cutting of turbulent eddies, were clearly measured at multiple receiving angles for advance ratios ranging from 1.44 to 0.48. As many as five observed harmonics were observed centered on multiples of the blade passing frequency (BPF). The far field noise was used to infer mean turbulence characteristics of the ingested boundary layer and downstream wake profile measurements were made phase-locked with blade position. Predictions of the far field noise were also presented and compared to the measurements. Significant findings follow:

- The rotor noise source is not a simple axially-aligned dipole and produces a significant normal component. Still, the measured noise at the lowest receiving angle is stronger than that measured in the rotor plane by as much as 20dB.

- As the ratio M_{tip}/M_{axial} increases, the haystacks become narrower and more symmetric about the BPF harmonics. This agrees with the theoretical observation of Glegg *et al.* (2012).

- A novel approach to inferring turbulence scales of the boundary layer has been presented in which the time-averaged spectra are used to calculate the lateral scale and the time-frequency distribution is used to calculate the streamwise (time) scale. This analysis shows, unexpectedly, that the time-scale of the turbulence interacting with the rotor decreases as the advance ratio drops, while the lateral scale of the turbulence remains almost constant. Further work is needed to extend and corroborate these findings. Wind tunnel experiments to directly measure the unsteady upwash and correlations in the rotating frame are scheduled for Summer 2013.

- Blade wake profiles were measured 0.64 chords downstream of the trailing edge of the blades. The phase-locked average turbulence quantities show increased mixing with the boundary layer as the rotor thrust is increased. Mean velocity profiles show significant velocity in the direction of the rotor rotation.

- Predictions have been compared to measurement for a thrusting (J=0.72) and non-thrusting case (J=1.44). The predicted spectra are very similar to the measured results. An equivalent number of haystacks are observed in both the measurement and prediction. The predicted haystacks also narrow in the same way as measurement with increasing thrust. Although, there are slight differences between prediction and measurement most notably in the decay of the haystacking peaks with frequency.

Acknowledgments

The authors would like to thank the Office of Naval Research, in particular Drs. Ki-Han Kim and John Muench, for their support under grant N00014-10-1-0908 and N00014-10-1-0910. We would also like to acknowledge the collaboration with Dr. Jason Anderson and Mr. Ryan Catlett at NSWCCD. The authors wish to thank the faculty and staff of the Applied Research Lab at Penn State University for helping to balance the rotor, in particular, Jim Mickey and Bill Straka as well as Eric Paterson, now Department Head of Aerospace and Ocean Engineering at Virginia Tech. Finally, we would like to acknowledge the hard work and dedication of the staff in Virginia Tech's Aerospace and Ocean Engineering Department, specifically: Andy Tawney and James Lambert who aided the authors in the design process and did a wonderful job machining the rotor, Bill Oetjens our tunnel engineer, Scott Patrick who designed and printed our inflow microphone stands, and Mark Montgomery our electrical engineer.

References

Awasthi, M, 2012, "High Reynolds Number Turbulent Boundary Layer Flow over Small Forward Facing Steps", Master's Thesis, AOE Department, Virginia Tech, Avail: http://scholar.lib.vt.edu/theses/available/etd-06292012-120614/.

Blake, W, *Mechanics of Flow Induced Sound and Vibration*, Wiley, New York, 1986.

Catlett M R, Anderson, J M, and Stewart D O, "Aeroacoustic Response of Propellers to Sheared Turbulent Inflows", 18th AIAA/CEAS Aeroacoustics Conference, Colorado Springs, CO, June 4-6, 2012, AIAA-2012-2137.

Devenport,W J, Burdisso, R A, Borgoltz, A, Ravetta, P A, Barone, M F, Brown, K A, and Morton, M A, 2013, "The Kevlar-Walled Anechoic Wind Tunnel", *Journal of Sound and Vibration*, http://dx.doi.org/10.1016/j.jsv.2013.02.043i

Forest, J, 2012, "The Wall Pressure Spectrum of High Reynolds Number Rough-Wall Turbulent Boundary Layers", Master's Thesis, AOE Department, Virginia Tech, Avail: http://scholar.lib.vt.edu/theses/available/etd-02022012-152048/.

Glegg, S A L, Morton, M, Devenport, W, "Rotor Inflow Noise Caused by a Boundary Layer: Theory and Examples", 18th AIAA/CEAS Aeroacoustics Conference, Colorado Springs, CO, June 4-6, 2012, AIAA-2012-2263.

Glegg, S A L, Kawashima, E, Lachowski, F, Devenport, W, and Alexander, N, "Inflow Distortion Noise in a Non Axisymmetric Flow", 19th AIAA/CEAS Aeroacoustics Conference, Berlin, DE, May 27-29, 2013. *To be presented*.

Hanson, D B, 1974 "Spectrum of Rotor Noise Caused by Atmospheric Turbulence", *Journal of the Acoustical Society of America*, vol. 56(1), pp. 110-126.

Hersh, A S, Soderman, P T, and Hayden R E, 1974, "Investigation of Acoustic Effects of Leading-Edge Serrations on Airfoils", *Journal of Aircraft*, vol. 11(4), pp. 197-202.

Paterson, R W, Vogt, P G, Fink, M R, and Munch C L, 1973, "Vortex Noise of Isolated Airfoils", *Journal of Aircraft*, vol. 10(5), pp. 296-302.

Majumder S and Peake N, 1998, "Noise Generation by the Interaction between Ingested Turbulence and a Rotating Fan", *Journal of Fluid Mechanics*, vol. 359, pp. 181-216.

Morton, M A, 2012, "Rotor Inflow Noise Caused by a Boundary Layer: Inflow Measurements and Noise Predictions", Master's Thesis, AOE Department, Virginia Tech, Avail: http://scholar.lib.vt.edu/theses/available/etd-08102012-103032/.

Morton M, Devenport W, Alexander W N, Glegg S A L, and Borgoltz A, "Rotor Inflow Noise Caused by a Boundary Layer: Inflow Measurements and Noise Predictions", 18th AIAA/CEAS Aeroacoustics Conference, Colorado Springs, CO, June 4-6, 2012, AIAA-2012-2120.

Sevik, M, “Sound Radiation from a Subsonic Rotor Subjected to Turbulence”, 1971, NASA SP 304.

Stephens D and Morris C, 2009, “Sound Generation by a Rotor Interacting with a Casing Turbulent Boundary Layer”, *AIAA Journal*, vol. 47, pp. 2698-2708.

Wojno J, Mueller T and Blake W, 2002, “Turbulence Ingestion Noise, Part 1: Experimental Characterization of Grid-Generated Turbulence”, *AIAA Journal*, vol. 40, pp. 16-25.

Wojno J, Mueller T and Blake W, 2002, “Turbulence Ingestion Noise, Part 2: Rotor Aeroacoustic Response to Grid Generated Turbulence”, *AIAA Journal*, vol. 40, pp. 26-32.

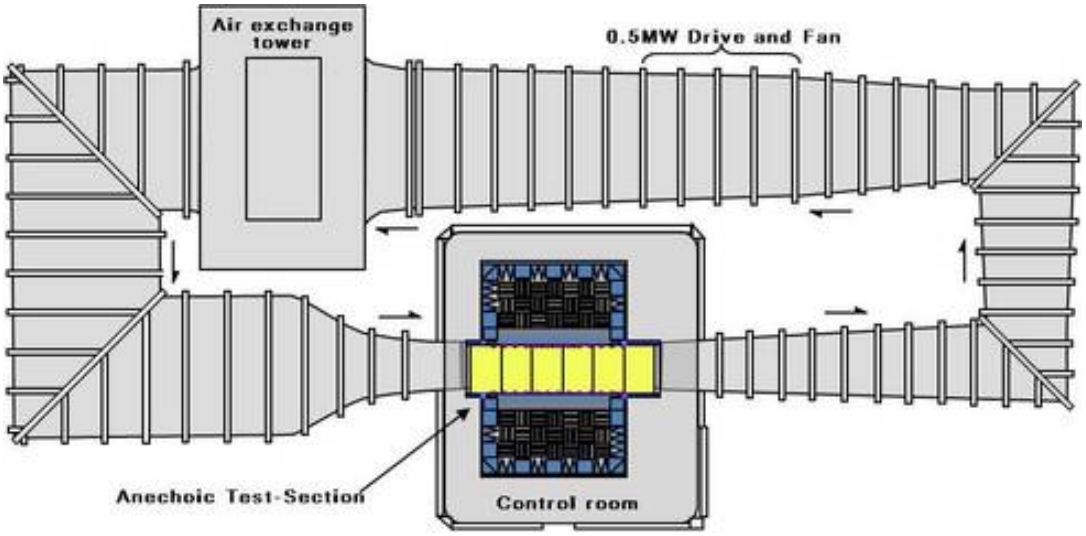

Figure 1a. Schematic of the Virginia Tech Stability Wind Tunnel (from Virginia Tech AOE Dept. website).

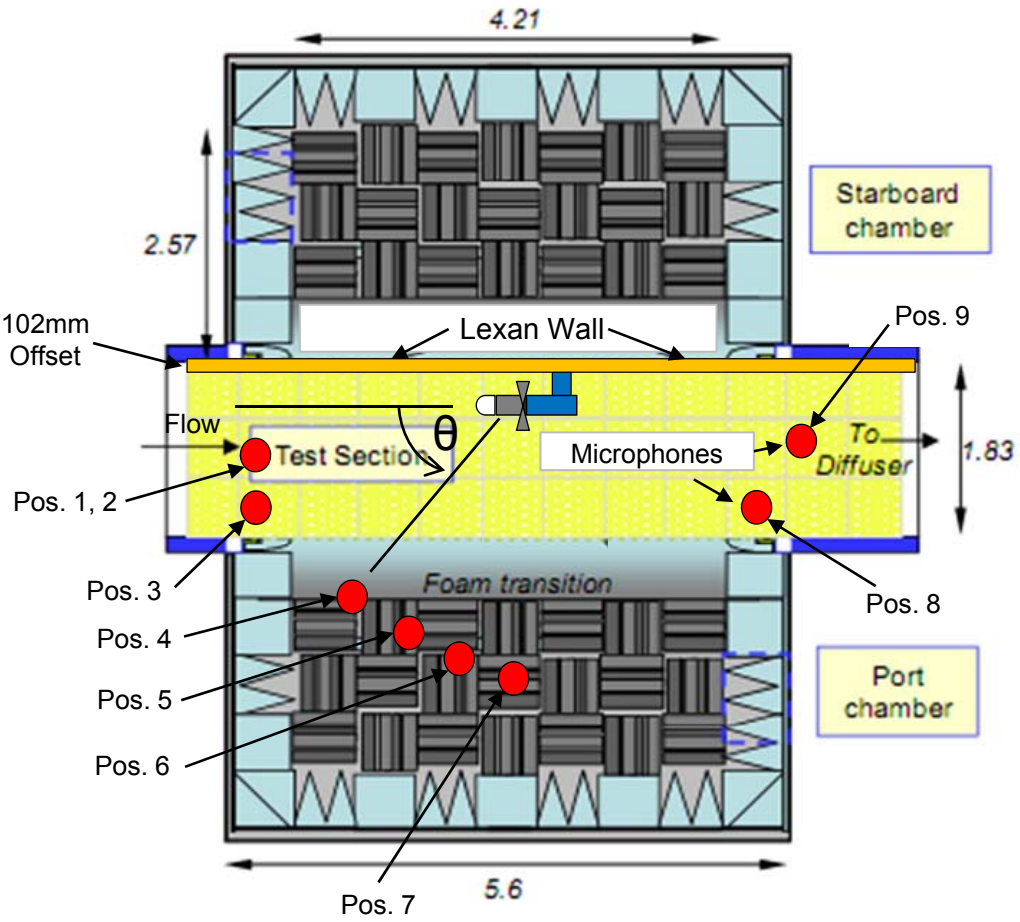

Figure 1b. Detail view showing test section and rotor and microphone configuration.

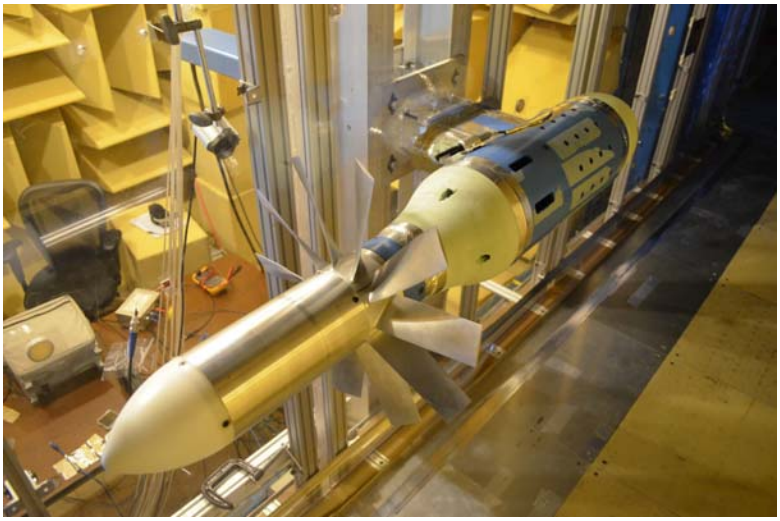

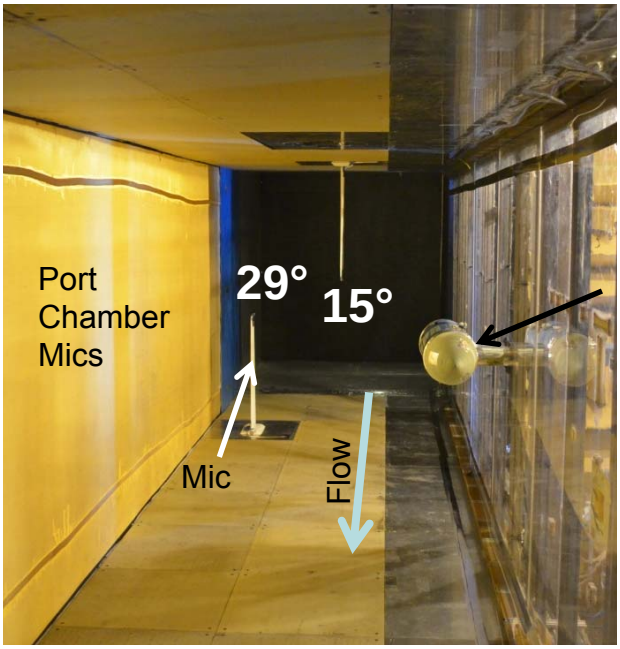

a) b)

Figure 2. a) Rotor and b) view of test section and inflow microphones.

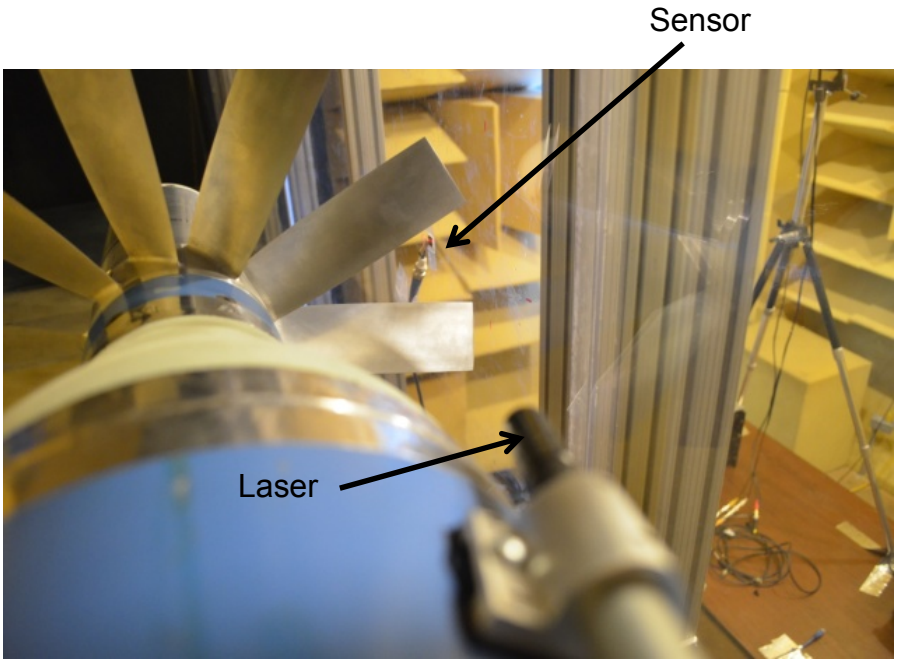

Figure 3. Laser/photodiode system used to measure blade position.

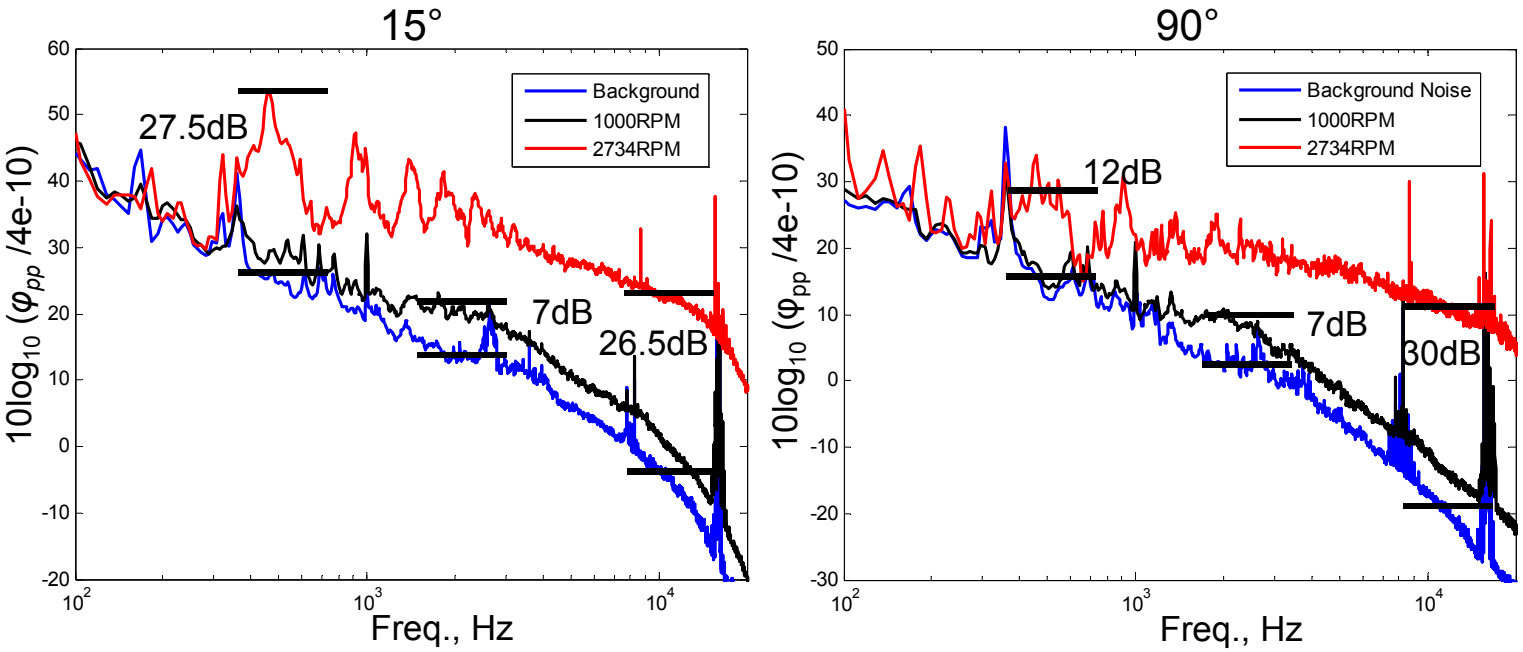

a) b)

Figure 4. Signal-to-noise ratio at U_∞=15m/s for microphones at a) θ=15° and b) θ=90°

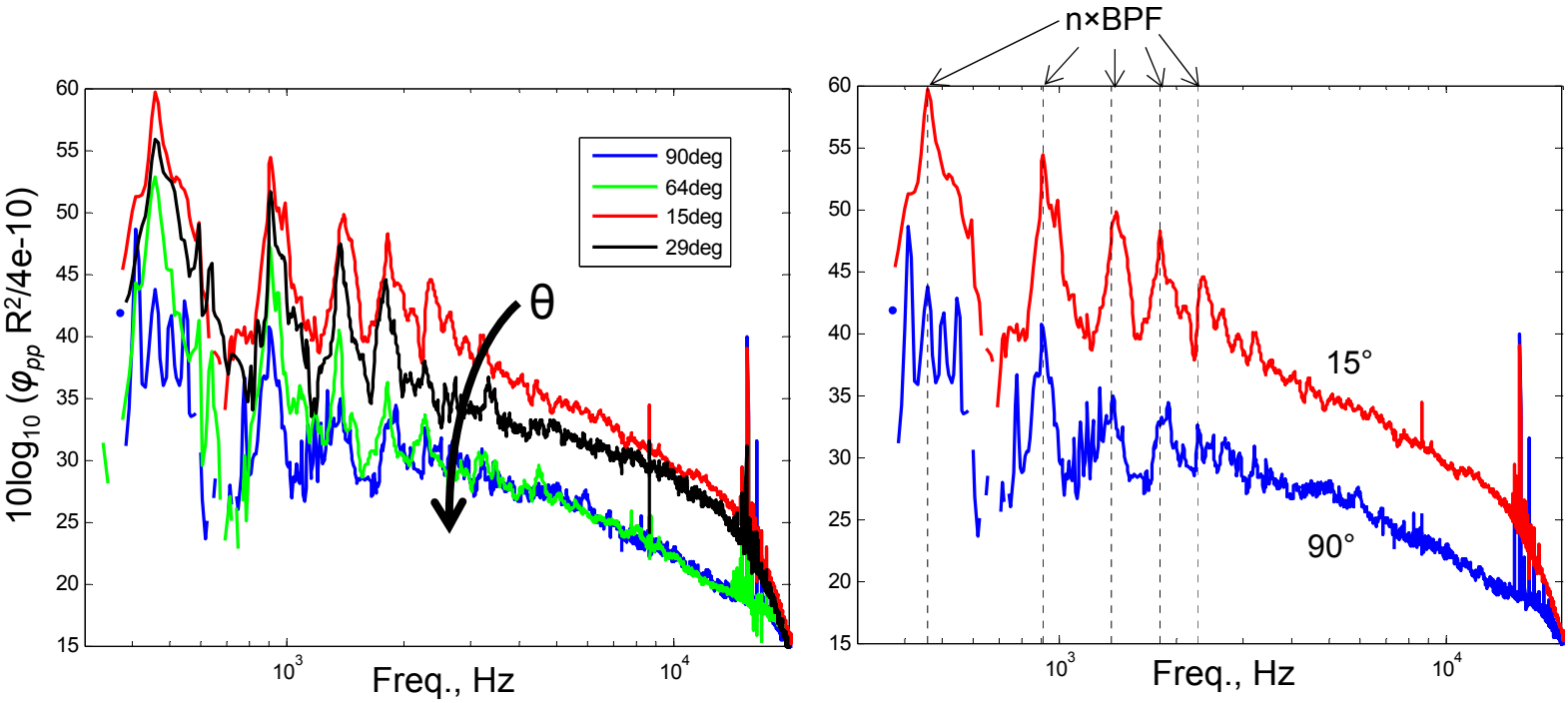

a) b)

Figure 5. Source directivity for U_∞= 15m/s, 2734RPM

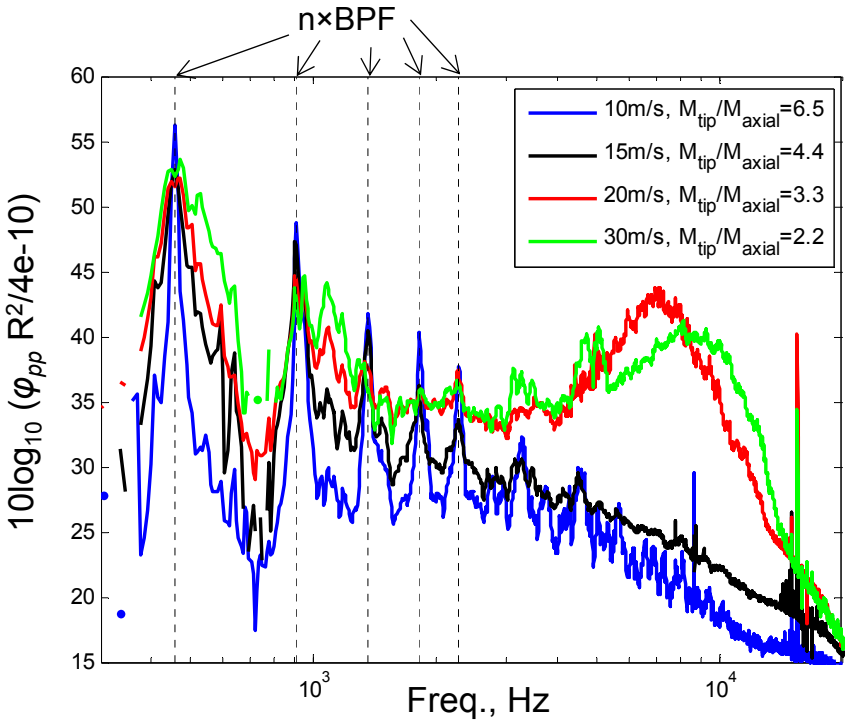

Figure 6. Rotor noise with variation of M_{tip}/M_{axial} measured at θ=64°

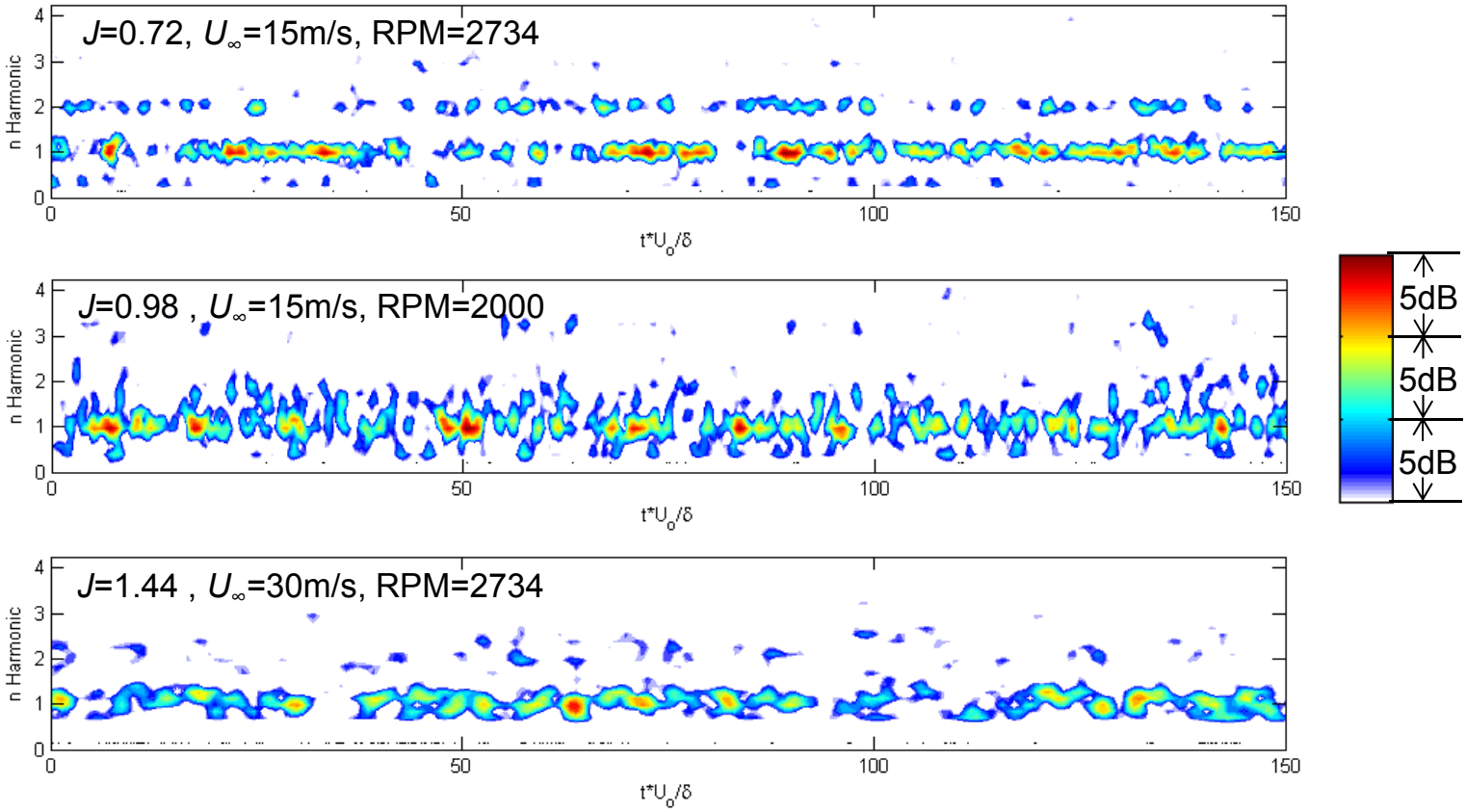

Figure 7. Spectrogram of noise recorded at θ=64° for several operating conditions

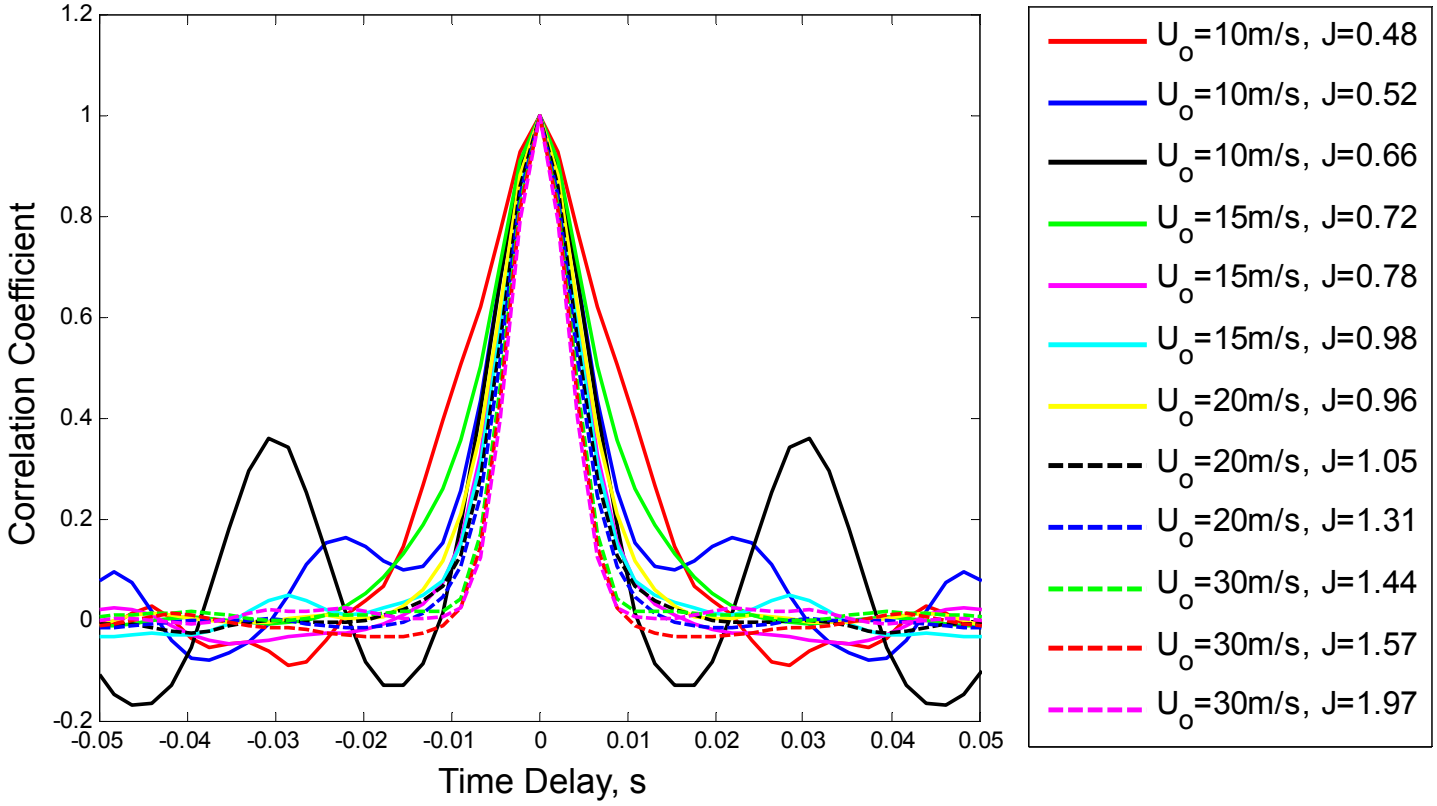

Figure 8. Autocorrelation of time-frequency distribution recorded at BPF

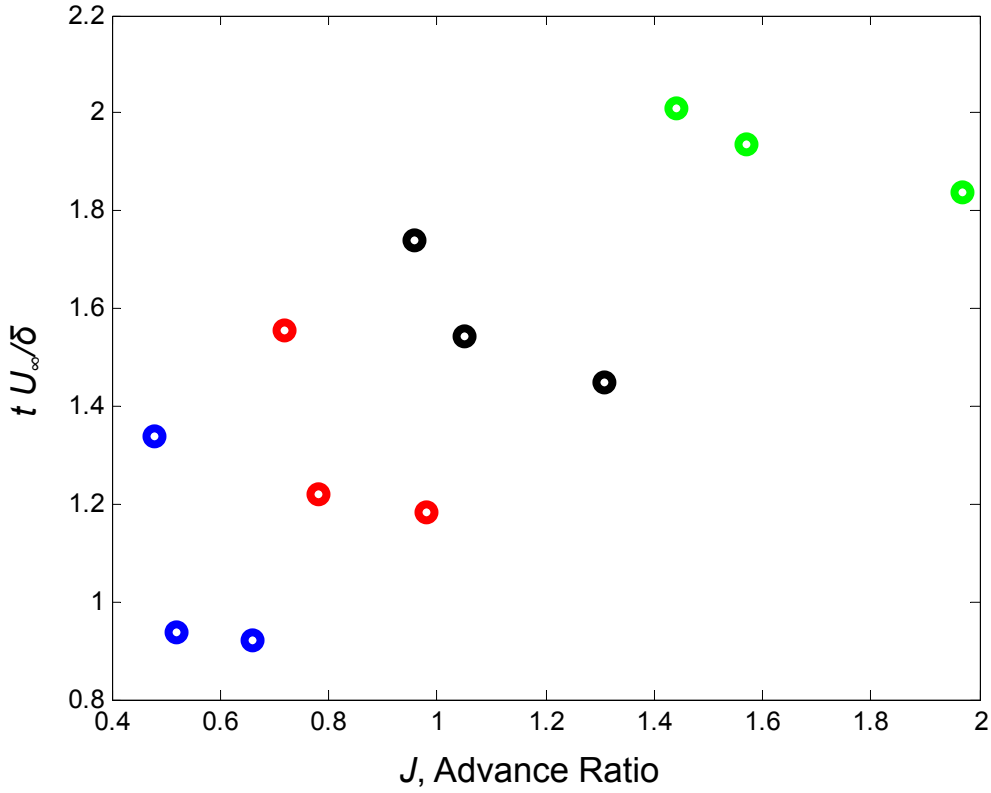

Figure 9. Normalized integral timescale of noise signal at BPF

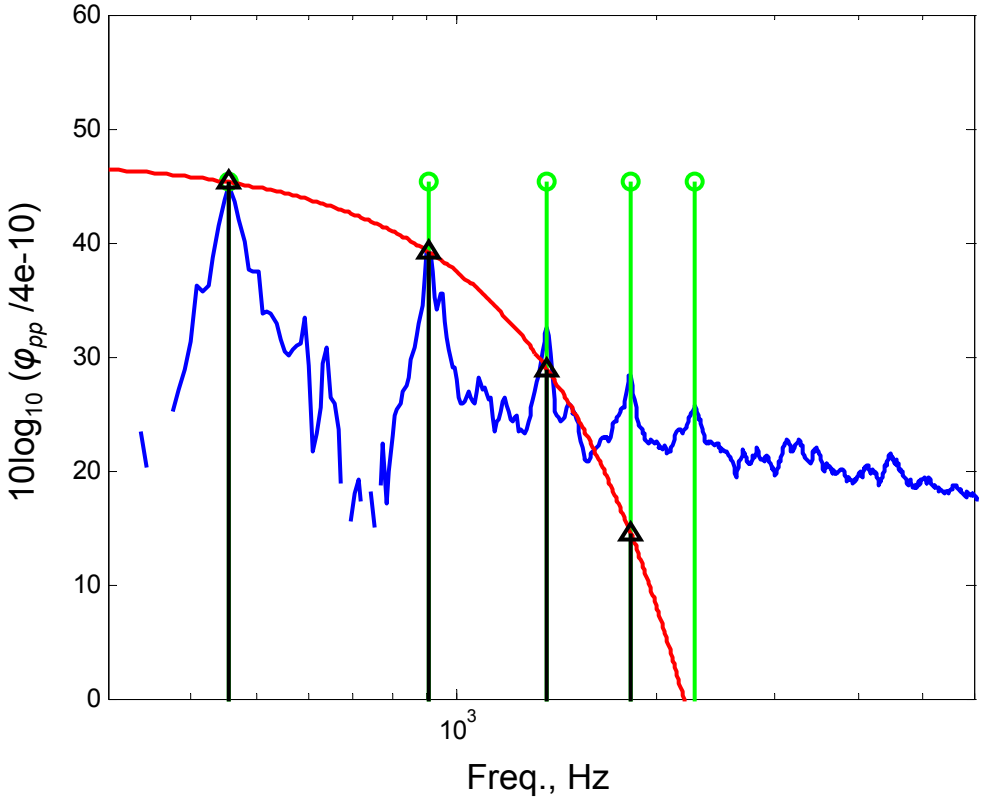

Figure 10. Noise at U_∞=15m/s, 2734RPM, θ=64° compared to the Fourier transform of a periodic train of impulses and Guassian functions

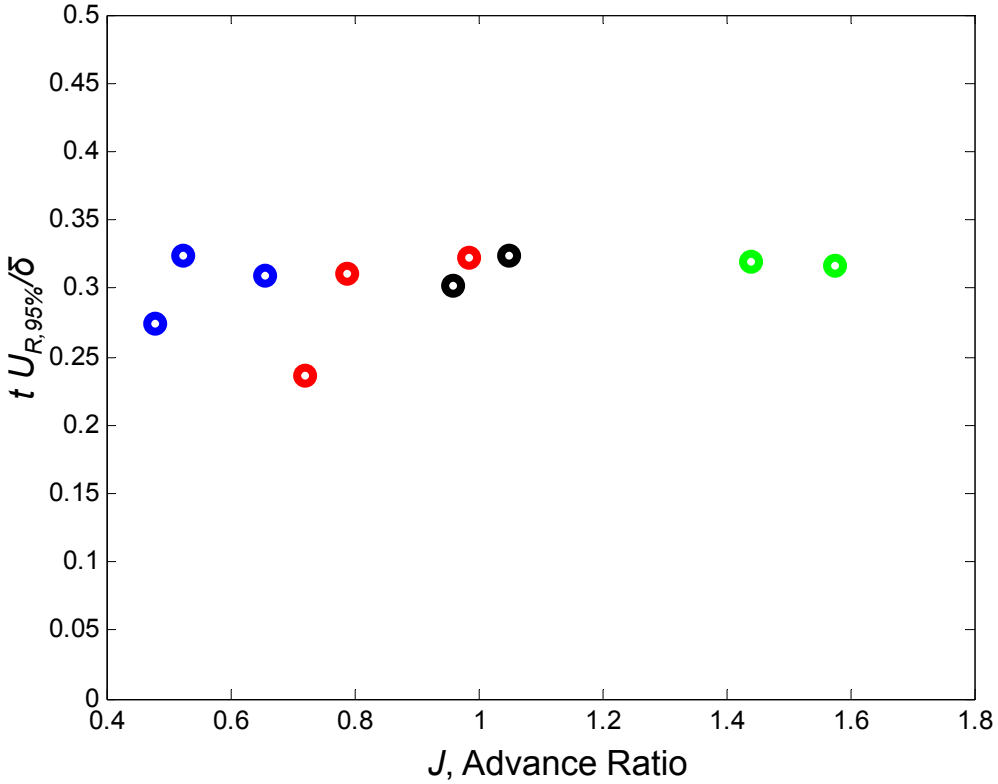

Figure 11. Lateral normalized timescale determined from halfwidth of fitted Guassian functions

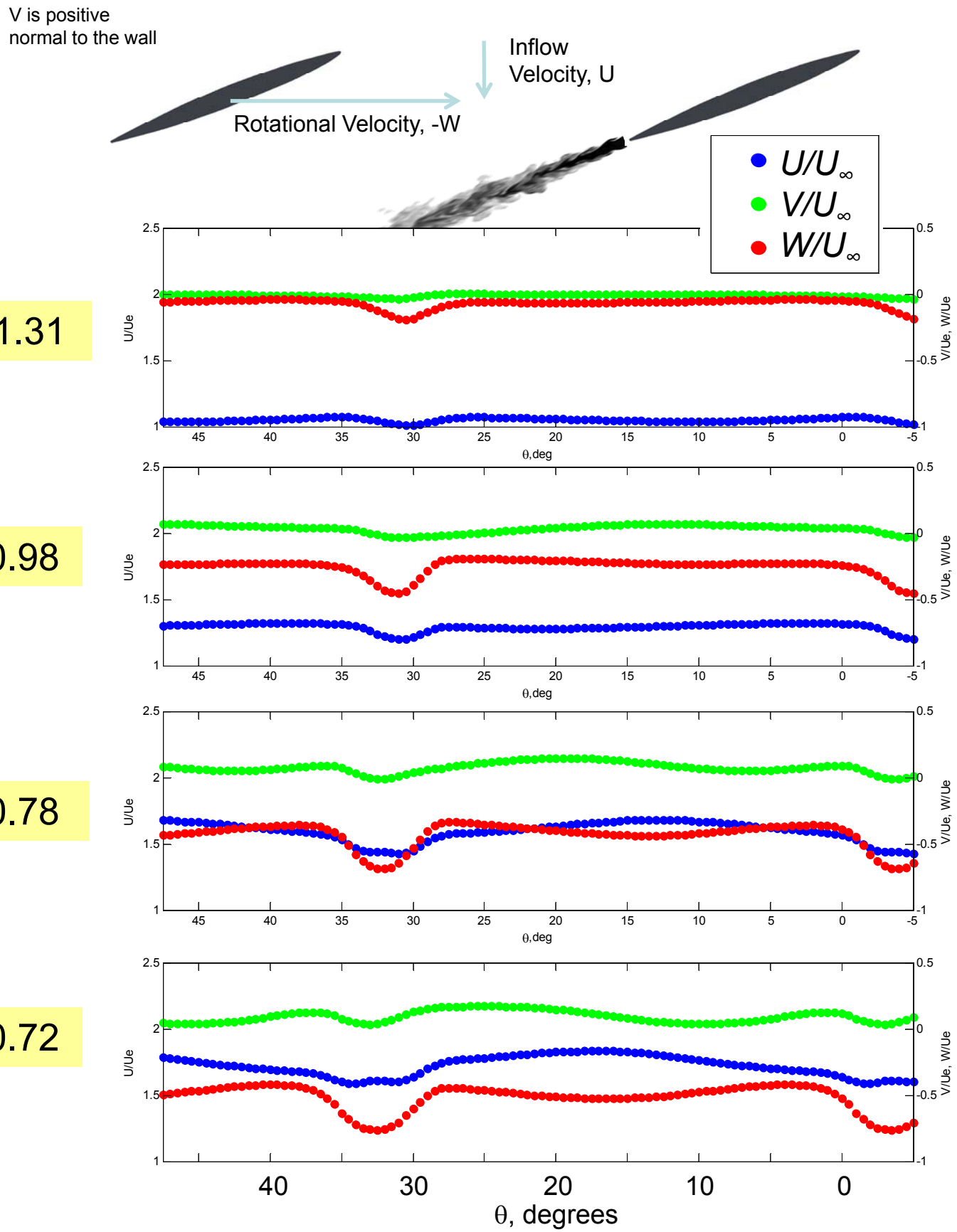

Figure 12. Mean velocity components measured in rotor wake

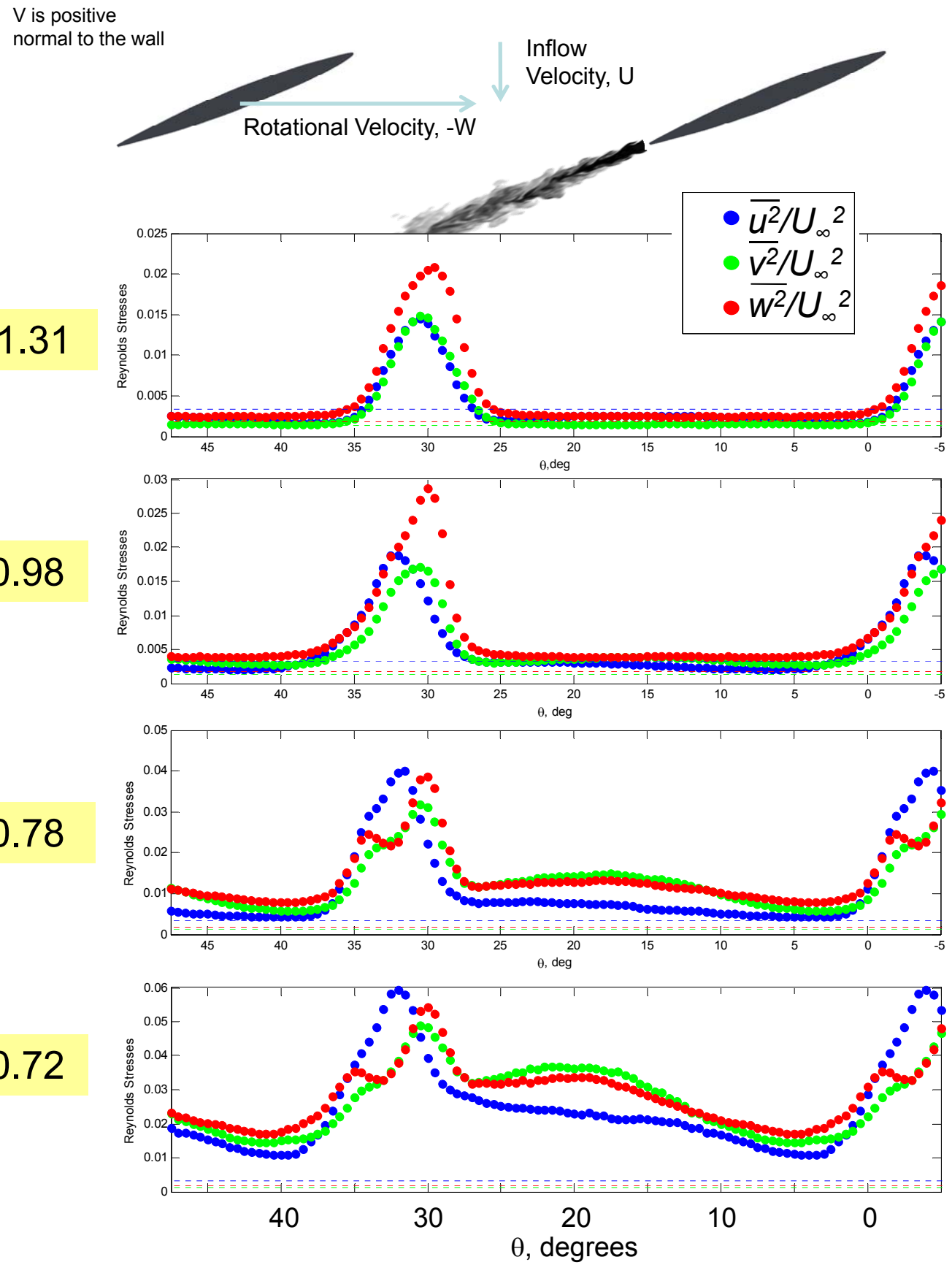

Figure 13. Reynolds normal stresses measured in rotor wake (lines indicate undisturbed boundary layer values)

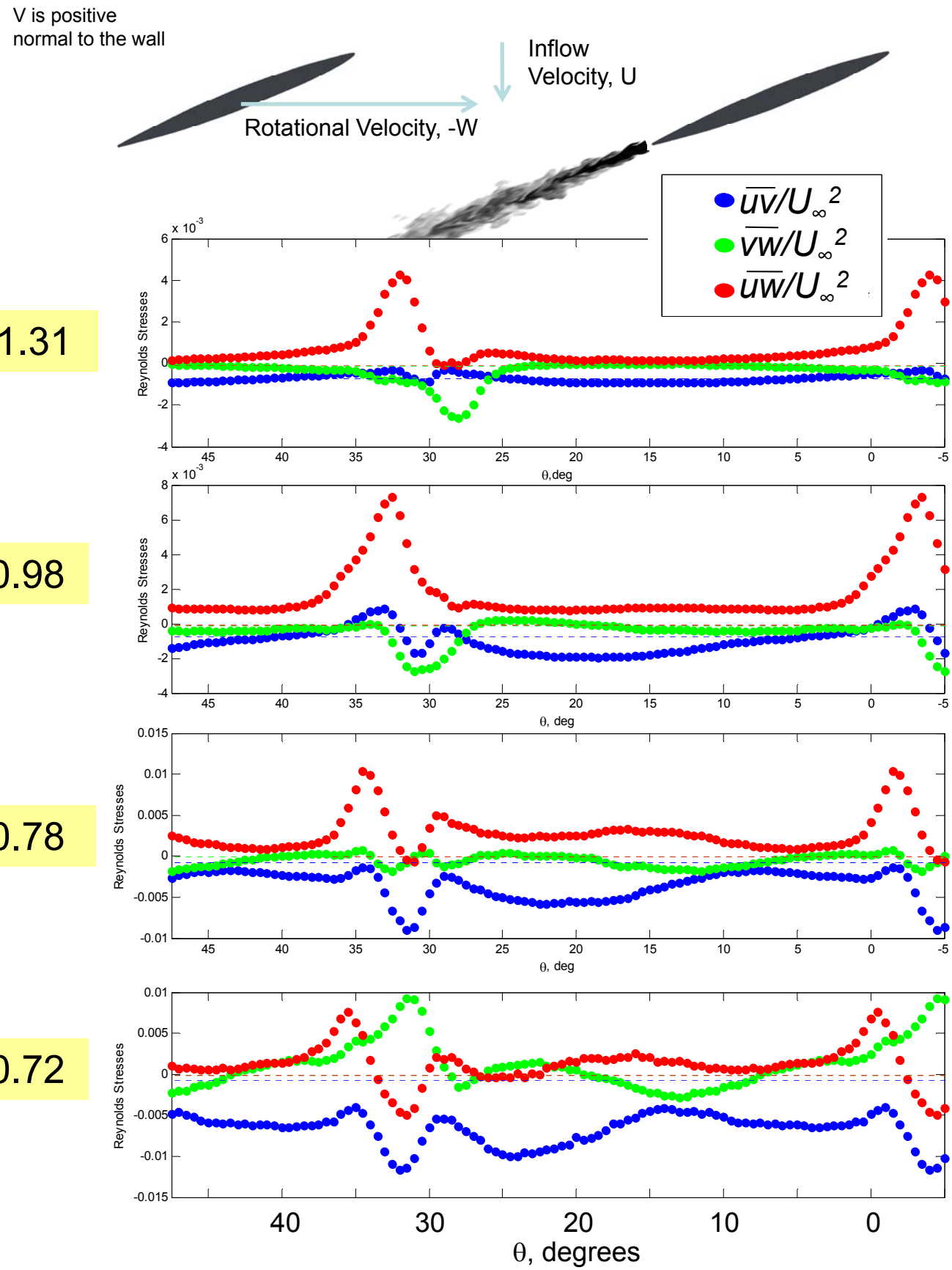

Figure 14. Reynolds shear stresses measured in rotor wake (lines indicate undisturbed boundary layer values)

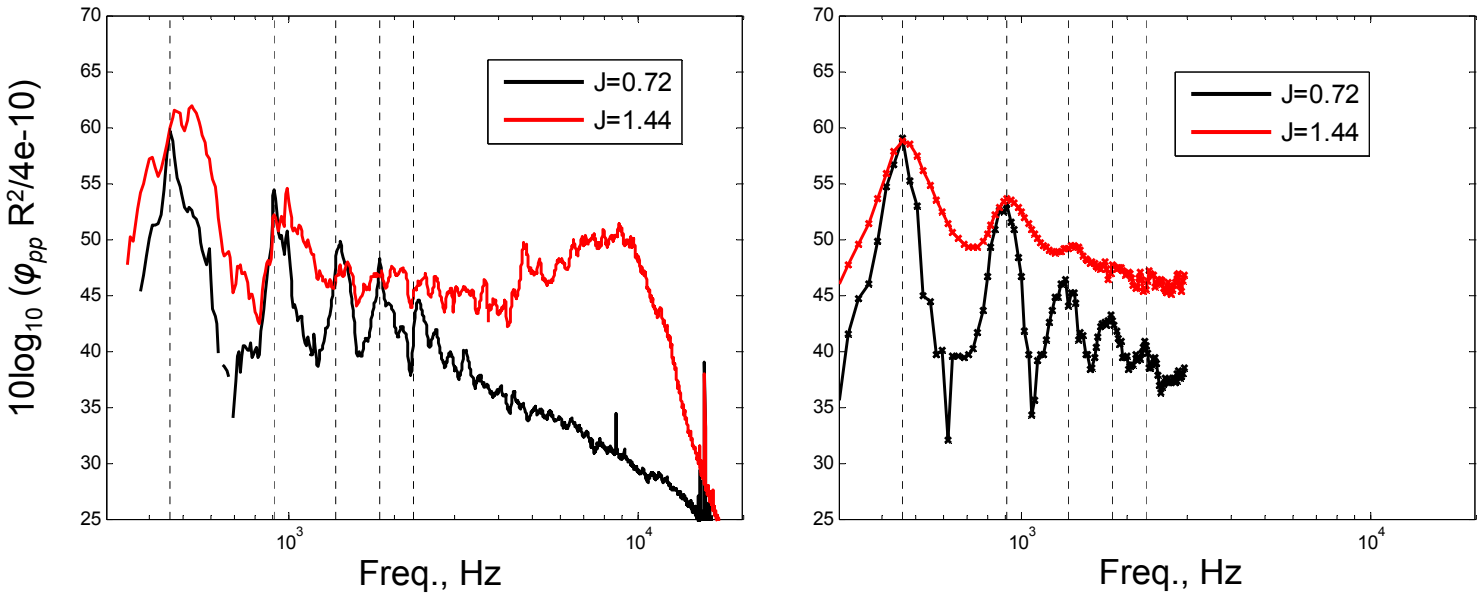

Figure 15. a) Measurement compared to b) predictions of noise for J=1.44, U_∞=30m/s, 2734RPM, θ=15° and J=0.72 ,U_∞=15m/s, 2734RPM, θ=15°